Conditional Dynamics in Heterodyne Detection of Superradiant Lasing with Incoherently Pumped Atoms

Huihui Yu,[1] Yuan Zhang,[1,2,*] Qilong Wu,[1] Chong-Xin Shan,[1,2,†] and Klaus Mølmer[3,‡]
[1]Henan Key Laboratory of Diamond Optoelectronic Materials and Devices, Key Laboratory of Material Physics Ministry of Education, School of Physics and Microelectronics, Zhengzhou University, Daxue Road 75, Zhengzhou 450052, China
[2]Institute of Quantum Materials and Physics, Henan Academy of Sciences, Mingli Road 266-38, Zhengzhou 450046, China
[3]Niels Bohr Institute, University of Copenhagen, Blegdamsvej 17, 2100 Copenhagen, Denmark

(Received 4 December 2022; revised 7 June 2024; accepted 18 June 2024; published 12 August 2024)

In this Letter, we use quantum trajectory theory to simulate heterodyne detection of narrow bandwidth superradiant lasing from an incoherently excited atomic ensemble. To this end, we describe the system dynamics and account for stochastic measurement backaction by second-order mean-field theory. Our simulations show how heterodyne measurements break the phase symmetry, and initiate the atomic coherence with a random phase and a long temporal phase coherence. More importantly, our theory allows direct simulation of experimental procedures for extraction of spectral information which do not lend themselves to evaluation with the quantum regression theorem.

DOI: 10.1103/PhysRevLett.133.073601

Introduction—Atomic clocks are used for international time standards, national time services, satellite navigation systems [1], and studies of general relativity [2]. By exploring optical ($\sim 10^5$ GHz) rather than microwave (∼GHz) transitions [3], the optical clocks improve the performance by orders of magnitude, and are thus the subject of considerable attention [4]. In particular, optical lattice clocks are extensively pursued because they mitigate Doppler broadening and collisional effects, and also provide better signal-to-noise ratio with more atoms [5]. In 2009, D. Meiser *et al.* proposed that optical lattice clocks can be explored to realize a superradiant laser with an ultranarrow spectrum, in which the atomic collective decay is compensated by continuous incoherent atomic pumping [6]. Owing to the high application potential of radiation with exceptional frequency stability [4], the superradiant laser has been further studied both theoretically [7–9] and experimentally [10–13].

In the theoretical studies, optical spectra are often calculated by quantum regression theorem (QRT) [14]. This is valid for the average power spectrum, but it glosses over the intricate interplay between the noisy measurement record, the induced backaction, and the transient behaviour of the emitter. Glauber's theory of photodetection [15] emphasizes how photon counting is accompanied by the annihilation of radiation quanta, which triggers subsequent transient correlations known as bunching and antibunching. Similar backaction mechanisms are at play in field amplitude measurements where they are responsible for temporal correlations in, e.g., heterodyne detection records, which characterize the frequency contents of the signal [12,13,16]. The QRT, in particular, does not quantitatively account for the fluctuations in spectral parameters as obtained by fitting the power spectra within a finite number of measurements.

In this Letter, we demonstrate that a theoretical description based on stochastic mean-field theory can be used to simulate the evolution of the atomic ensemble and the extraction of frequency from noisy heterodyne signals. We find that a second-order mean-field approach is necessary to account for the measurement backaction, and that the backaction introduces a random initial phase of the optical coherence, which rules the outcome of subsequent measurements. Our approach permits application and hence analysis of fitting procedures as used to extract optical frequencies in experiments, and it offers also insights into the microscopic dynamics that are not offered by the QRT.

System and model—To illustrate the above points, we study a specific system with tens of thousands of calcium atoms inside an optical cavity [Fig. 1(a)]. The atoms are initially prepared in the 4^3P_1 excited state by a complex process involving transfer from a magneto-optical trap to an optical lattice trap [17,18] (see Fig. S1 of the Supplemental Material [19]). Normally, the preparation step can be modeled effectively by an incoherent pumping rate [6,8,20]. The narrow-band intercombination transition to the 4^1S_0 ground state couples resonantly with the cavity, leading to the superradiance [Fig. 1(b)]. The superradiant pulses of such a system have been studied experimentally [18], and the influence of the atom-cavity coupling, the frequency detuning, and the incoherent pumping has been

*Contact author: yzhuaudipc@zzu.edu.cn
†Contact author: cxshan@zzu.edu.cn
‡Contact author: klaus.molmer@nbi.ku.dk

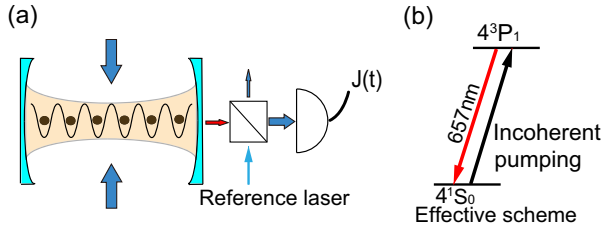

FIG. 1. System schematics and atomic energy diagram. Panel (a) illustrates tens of thousands of calcium atoms trapped in an optical lattice inside an optical cavity. The field generated by the incoherently pumped atoms leaks out of the cavity, and is measured by heterodyne detection. Panel (b) shows the simplified energy scheme with the atoms incoherently pumped to the 4^3P_1 excited state (black arrow), and the Purcell-enhanced and collective decay of the excited atoms to the 4^1S_0 ground state by emission into the optical cavity mode (red arrow).

analyzed theoretically [25]. However, in the following, we shall examine the transient and steady-state superradiance, with a focus on the dynamics conditioned on the heterodyne detection and the accompanying frequency determination.

To describe the system's conditional dynamics, we have reformulated the stochastic quantum master equation developed in our previous work [21], and we have supplemented the QuantumCumulants.jl package [22] with codes that automatically derive and solve the stochastic mean-field equations (see Secs. S1 and S2 of the Supplemental Material [19]). The QuantumCumulants.jl package permits mean-field calculations to any specified order, but we concentrate on the second order, which leads to a manageable number of differential equations, and also accounts for both atom-atom and atom-photon correlations. In our theory, the cavity mode is modeled as a quantum harmonic oscillator with a frequency $\omega_c = 2\pi \times 456.6$ THz and a photon damping rate $\kappa = 2\pi \times 1.13$ MHz. More than $N = 5 \times 10^4$ atoms are modeled as two-level systems with a transition frequency $\omega_a = \omega_c$, and with decay, dephasing, and incoherent pumping rates $\gamma = 2\pi \times 0.375$ kHz, $\chi = 2\pi \times 0.016$ Hz, and $\eta = 2\pi \times 20$ kHz. The cavity couples to the atoms with a strength $g = 2\pi \times 0.73$ kHz. The output from the right mirror of the cavity is mixed with a reference laser with frequency $\omega_l = \omega_c + 2\pi \times 1$ MHz, and their interference signal is measured by photodetectors with a counting efficiency ξ. The photocurrent

$$J(t) = \sqrt{2\xi\kappa}\mathrm{Re}[e^{-i\omega_l t}\langle\hat{a}^\dagger\rangle(t)] + dW/dt \tag{1}$$

is governed by the expectation value of the cavity field amplitude $\langle\hat{a}^\dagger\rangle$ but is dominated by the shot-noise term dW/dt at short time, where the random number dW follows a normal distribution with a mean $E[dW] = 0$ and a variance $dW^2 = dt$ [23] (with dt as the simulation step).

We adopt two complementary pictures to illustrate the collective dynamics of the atomic ensemble. The first picture uses the collective spin vector $\mathbf{A} = \sum_{i=x,y,z} A_i \mathbf{e}_i$, where $A_x = (N/2)(\langle\hat{\sigma}_1^{12}\rangle + \langle\hat{\sigma}_1^{21}\rangle)$, $A_y = (iN/2)(\langle\hat{\sigma}_1^{12}\rangle - \langle\hat{\sigma}_1^{21}\rangle)$, $A_z = (N/2)(2\langle\hat{\sigma}_1^{22}\rangle - 1)$, and $\mathbf{e}_i$ are the unit vectors of the Cartesian coordinate system (see Sec. S2 of the Supplemental Material [19] for more details). Here, $\hat{\sigma}_k^{21}$, $\hat{\sigma}_k^{12}$ are transition operators of the kth atom between the ground and excited state (labeled by 1,2, respectively), and $\hat{\sigma}_k^{22}$ is the projection operator on the excited state. Thus, the expectation values $\langle\hat{\sigma}_1^{12}\rangle$ and $\langle\hat{\sigma}_1^{21}\rangle$ are the atomic coherences, and $\langle\hat{\sigma}_1^{22}\rangle$ is the excited state population of any individual atom, represented by the first one. For the atomic ensemble in pure product states, the collective spin vector traces a sphere of radius $N/2$, where the south (north) pole represents the atomic ensemble in the fully ground (excited) state.

The second picture uses the Dicke states $|J, M\rangle$, where the positive integer or half integers J, M in the range $J \le N/2$, $-J \le M \le J$ describe the degree of symmetry and excitation of the two-level systems ensemble [26], respectively. The influence of various processes in the master equation can be conveniently visualized in the space of Dicke states [27,28], and here we shall employ this space to represent the results obtained by the mean-field approach. Since the Dicke states are defined as eigenstates of the collective spin operators $\hat{J}_z, \hat{J}^2$: $\hat{J}_z|J, M\rangle = M|J, M\rangle$, $\hat{J}^2|J, M\rangle = J(J-1)|J, M\rangle$, we can calculate the mean value of M and J through $\bar{M} = \langle\hat{J}_z\rangle$, $\bar{J}(\bar{J}-1) = \langle\hat{J}^2\rangle$ (see Sec. S2 of the Supplemental Material [19] for more details).

The full set of equations is detailed in Sec. S4 of the Supplemental Material [19]. However, to explain the numerical results below, we shall reproduce here the equations for the field amplitude

$$\begin{aligned}\partial_t\langle\hat{a}^\dagger\rangle = {} & i\tilde{\omega}_c\langle\hat{a}^\dagger\rangle + iNg\langle\hat{\sigma}_1^{21}\rangle \\ & + (dW/dt)\sqrt{\xi\kappa/2}e^{i\omega_l t}(\langle\hat{a}^\dagger\hat{a}\rangle - \langle\hat{a}^\dagger\rangle\langle\hat{a}\rangle) \\ & + (dW/dt)\sqrt{\xi\kappa/2}e^{-i\omega_l t}(\langle\hat{a}^\dagger\hat{a}^\dagger\rangle - \langle\hat{a}^\dagger\rangle^2),\end{aligned} \tag{2}$$

and the atomic coherence

$$\begin{aligned}\partial_t\langle\hat{\sigma}_1^{21}\rangle = {} & i\tilde{\omega}_a\langle\hat{\sigma}_1^{21}\rangle + ig(\langle\hat{a}^\dagger\rangle - 2\langle\hat{a}^\dagger\hat{\sigma}_1^{22}\rangle) \\ & + (dW/dt)\sqrt{\xi\kappa/2}e^{-i\omega_l t}(\langle\hat{a}^\dagger\hat{\sigma}_1^{21}\rangle - \langle\hat{a}^\dagger\rangle\langle\hat{\sigma}_1^{21}\rangle) \\ & + (dW/dt)\sqrt{\xi\kappa/2}e^{i\omega_l t}(\langle\hat{a}\hat{\sigma}_1^{21}\rangle - \langle\hat{a}\rangle\langle\hat{\sigma}_1^{21}\rangle),\end{aligned} \tag{3}$$

where the complex frequencies are defined as $\tilde{\omega}_c = \omega_c + i\kappa/2$, $\tilde{\omega}_a = \omega_a + i(\eta + \gamma + 2\chi)/2$. The first-order mean-field approach applies the approximation $\langle\hat{o}\,\hat{p}\rangle \approx \langle\hat{o}\rangle\langle\hat{p}\rangle$ for any operators $\hat{o}$, $\hat{p}$. Under this approximation, the factors multiplying the stochastic term dW in the second and third line of Eqs. (2) and (3) vanish. Thus,

the measurement backaction is completely missed. Furthermore, since the system is incoherently pumped and the field amplitude $\langle \hat{a}^\dagger \rangle$ and the atomic coherence $\langle \hat{\sigma}_1^{21} \rangle$ are initially zero, they will remain vanishing for all time. To remedy the shortcoming of such a treatment, it has been proposed to introduce a weak initial perturbation to the cavity field or the atoms [18,25,29,30] (Fig. S7 of the Supplemental Material [19]). However, as shown below, such *ad hoc* breaking of the phase symmetry is not needed when the backaction due to heterodyne measurements is taken into account.

Going beyond the above treatment, we may retain second-order operators by their explicit mean values, and apply the approximation $\langle \hat{o}\,\hat{p}\,\hat{q} \rangle \approx \langle \hat{o} \rangle \langle \hat{p}\,\hat{q} \rangle + \langle \hat{p} \rangle \langle \hat{o}\,\hat{q} \rangle + \langle \hat{q} \rangle \langle \hat{o}\,\hat{p} \rangle - 2\langle \hat{o} \rangle \langle \hat{p} \rangle \langle \hat{q} \rangle$ for higher moments of operators $\hat{o}, \hat{p}, \hat{q}$. As a result, the second and third lines of Eqs. (2) and (3) are preserved, and introduce finite values to the initially vanished first-order mean fields, i.e., a breaking of the phase symmetry by a rigorous physical mechanism. Although the finite first-order mean values may dominate over the stochastic terms in the subsequent evolution and diminish their effect on the conditional dynamics, the stochastic terms remain as a significant noise contribution to the photocurrent [see Eq. (1)].

In the following simulations, we study first the deterministic dynamics of the system in the absence of heterodyne detection (equivalent to setting $\xi = 0$), and we then investigate the conditional and stochastic dynamics in the presence of the measurement with a detector efficiency $\xi = 0.12$.

Deterministic dynamics—For reference, we first apply the cumulant mean-field approach to solve the deterministic master equation. Although the pulsed superradiant lasing has been demonstrated in several experiments [11,12,18], the continuous superradiant laser is still not achieved. Thus, we show results for pulsed incoherent pumping in Figs. 2(a) and 2(b), and we then predict the results for continuous incoherent pumping in Figs. 2(c) and 2(d).

For the pulsed excitation, the intracavity photon number (and hence the emitted signal) forms a pulse, which occurs at later time and has longer duration for systems with fewer atoms. In Fig. S4(a) in the Supplemental Material [19], we confirm that these results agree qualitatively with the observations in the experiment [18]. In the picture with the collective spin vector, the spin vector moves upward from the south pole to a point near the north pole, and then returns [inset of Fig. 2(a)], i.e., A_x, A_y vanish during the evolution of A_z. Accompanying this result, the mean cavity photon number remains finite, while the mean field amplitude vanishes at all time [see Fig. S5(a) of the Supplemental Material [19]]. In the Dicke states picture, the atomic ensemble progresses with increasing M values during the incoherent pumping, while the vanishing of the transverse spin components makes $\hat{J}^2 \simeq \hat{J}_z^2$, and hence the system explores states with $J = |M|$ along the boundaries

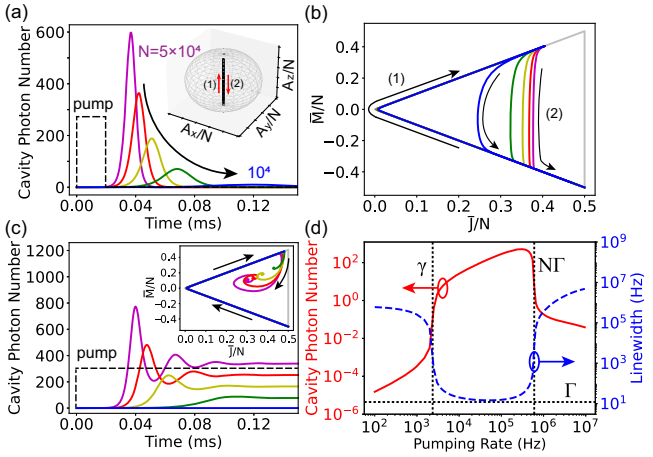

FIG. 2. Superradiant pulses (a),(b) and steady-state superradiance (c),(d) of incoherently pumped calcium atoms. Panels (a), (b) show the dynamics of the intracavity photon number (a) and the averaged Dicke state quantum numbers $\bar{J}, \bar{M}$ (b), which follow the two enumerated arrows for different numbers of atoms [$N = (1\text{–}5) \times 10^4$, arrows (2) from left to right]. In the panel (a), the pump pulse with a rate of $\eta = 2\pi \times 20$ kHz is indicated with a dashed line, and the inset shows the dynamics of the collective spin vector along the z axis for $N = 10^4$ atoms. Panel (c) shows similar results as the panels (a) and (b) but for the continuous incoherent pumping. Panel (d) shows the steady-state intracavity photon number (left axis) and the radiation linewidth (right axis), calculated by the QRT, as a function of the pumping rate for $N = 5 \times 10^4$ atoms. The horizontal short-dashed line represents the minimal linewidth of 12.02 Hz as determined by the Purcell-enhanced decay rate Γ, and the two vertical short-dashed lines represent the pumping at the spontaneous emission rate γ and the collective decay rate $N\Gamma$. For other parameters see Table S1 of the Supplemental Material [19].

of the Dicke triangle. Subsequently, the collective spin lowering operator causes a vertically downward exploration of Dicke states, leading to the pulsed superradiance [27,31,32] [Fig. 2(b)]. In these calculations with the second-order mean-field approach, the atom-atom correlations rather than a macroscopic mean dipole moment are responsible for the superradiance. In Fig. S6 of the Supplemental Material [19], we show the influence of the pumping rate and duration on the atomic ensemble dynamics and the superradiant pulses, providing further insights into the controllability of the superradiance.

Under the continuous incoherent pumping, the intracavity photon number oscillates in time before reaching its steady-state value [Fig. 2(c)]. The atomic ensemble undergoes an excitation dynamics similar to the pulsed case, but eventually explores and converges to states near the upper boundary of the Dicke triangle [see the inset of Fig. 2(c)]. In Fig. 2(d), we show the steady-state intracavity photon number $\langle \hat{a}^\dagger \hat{a} \rangle$ and the radiation linewidth $\delta\nu$ as a function of the pumping rate η. We have obtained the latter quantity by computing the steady-state spectrum with the QRT, and

then fitting the spectrum with a Lorentzian function. We see that as η increases from 10^2 Hz and surpasses the atomic decay rate $\gamma = 2\pi \times 375$ Hz, $\langle \hat{a}^\dagger \hat{a} \rangle$ increases gradually from 10^{-5} to 10^{-2}, and then rises abruptly to about 10^0 (the first threshold), while $\delta\nu$ decreases from almost 10^6 Hz to about 10^2 Hz. As η increases further and crosses over the collective decay rate $N\Gamma \approx 6 \times 10^6$ Hz (the second threshold), $\langle \hat{a}^\dagger \hat{a} \rangle$ first increases and then drops abruptly to 10^{-2}, while $\delta\nu$ approaches the Purcell-enhanced decay rate of a single atom $\Gamma = 4g^2/\kappa \approx 12$ Hz, and then rises abruptly above 10^6 Hz. When the minimal linewidth is achieved, the atomic ensemble explores the collective Dicke states with $0.1 < \bar{J}/N < 0.3$ and $\bar{M}/N$ which is slightly larger than zero [see Fig. S9(a) of the Supplemental Material [19]].

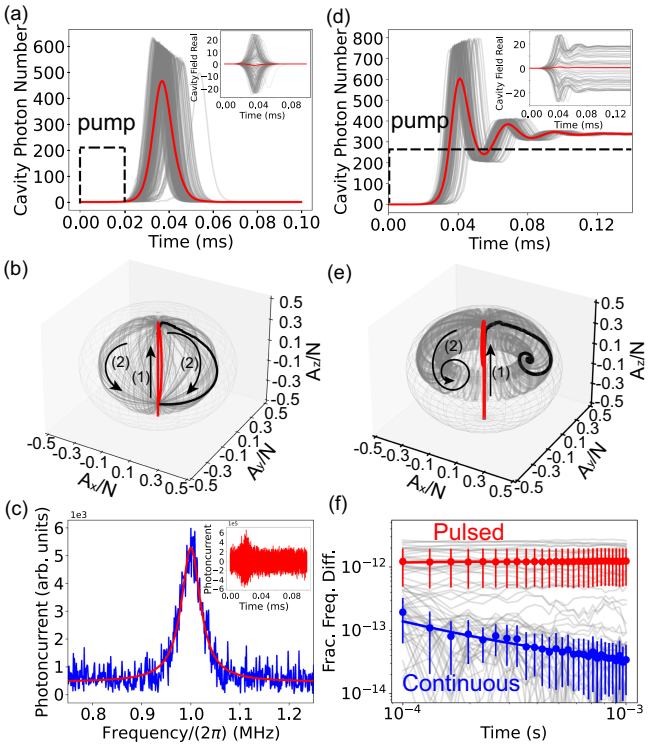

FIG. 3. Frequency measurement with heterodyne detection of pulsed (a)–(c) and steady-state (d)–(f) superradiance from 5×10^4 calcium atoms incoherently pumped with a rate of 20 kHz. The former is achieved by a pulsed pumping. Panels (a) and (b) show multiple trajectories (gray lines) and their average (red solid lines) of the intracavity photon number (a), the real part of the field amplitude (inset of a), and the collective spin vectors (b). The labels (1),(2) in the panel (b) mark the evolution at earlier and later time, respectively. Panel (c) shows the power spectrum obtained by the Fourier transform of the heterodyne signal in a single simulation (inset), and its fit by a Lorentzian function (red solid line). Panels (d),(e) show the same quantities as in the panels (a),(b) but for continuous pumping. Panel (f) shows the fractional frequency difference, as a function of the measurement time with pulsed (upper part) and steady-state superradiance (lower part), where the gray lines show the results for different simulations, and the dots and bars show the average and standard deviation. For other parameters see Table S1 of the Supplemental Material [19].

Conditional and stochastic dynamics in the presence of heterodyne detection—In Fig. 3 we present the conditional dynamics and the frequency measurement of the transient [(a)–(c)] and steady-state [(d)–(f)] superradiance from the pulsed and continuously pumped calcium atoms, respectively. In the former case, the intracavity photon number shows large variations in different simulations, but the average result almost reproduces the deterministic dynamics [Fig. 2(a)]. Importantly, the intracavity field amplitude develops nonvanishing values in individual simulations, while the average over many simulations vanishes [see the inset of Fig. 3(a) and Fig. S5(b) of the Supplemental Material [19]]. Since the field amplitude couples with the atomic coherence, the components A_x, A_y also acquire finite values, and the collective spin vector departs from the z axis and rotates on a spherical surface inside the sphere of radius $N/2$ [Fig. 3(b)], while the average over many trajectories almost recovers the deterministic dynamics along the z axis [Fig. 2(a)].

For each individual simulation, the instantaneous photocurrent is dominated by the white noise, but its envelope follows the real part of the intracavity field amplitude [inset of Fig. 3(c)]. Correspondingly, the power spectrum for each simulation shows a peak around $2\pi \times 1$ MHz, i.e., the frequency detuning of the reference laser to the optical cavity, with a width around $2\pi \times 28$ kHz, and can be well fitted by a Lorentzian function [Fig. 3(c)]. In Fig. S8 of the Supplemental Material [19], we have summarized the evolution of the fitted spectral parameters as a function of time, as may be directly verified in experiments.

In the case of constant pumping, the intracavity photon number shows strong variation in the transient dynamics while converging to the same steady-state values at longer time for all simulations [Fig. 3(d)]. The field amplitude, however, retains sizable variations in the steady state for different simulations (inset). The collective spin vector rotates and approaches steady state from different directions [Fig. 3(e)], in a manner such that the average over many simulations reproduces the deterministic dynamics. As the superradiant emission persists, the measurements for longer time improve the determination of the frequency, as shown by the lower blue dots and error bars in Fig. 3(f). In Fig. S9(b) of the Supplemental Material [19] we further verify that the spectral linewidth approaches 12 Hz as predicted by the QRT.

To evaluate the accuracy of the frequency estimation with the superradiant signal, we calculate the fractional frequency difference uncertainty, i.e. the relative difference between the extracted frequency and the atomic transition frequency, based on Lorentzian fits to the power spectrum of each simulated heterodyne photocurrent signal. In the case of

pulsed signals, the measurement uncertainty approaches a stable value about 10^{-12} [red curve of Fig. 3(f)], because the measurements at longer time are performed on the white noise, and carry no further information about the frequency. In the case of continuous pumping, to avoid the bias of early transient dynamics, we analyze only the part of the signal after the system has reached steady state. The fractional frequency uncertainty equals about 10^{-13} for the shortest integration time 0.1 ms [first blue dot in Fig. 3(f)], which is already about one order of magnitude smaller than in the pulsed case. As shown by the blue curve in Fig. 3(f), the fractional frequency difference scales as $9.7 \times 10^{-16}/\sqrt{\tau/s}$ with the probing time τ. Thus, a fractional frequency difference 10^{-15} could be potentially obtained with $\tau = 1$ s.

Discussions and conclusions—In summary, we have provided a precise description of heterodyne-based frequency measurements on the superradiance laser from incoherently pumped atoms. We have demonstrated that the frequency precision can be significantly improved with the continuous superradiance as compared to the case of pulsed superradiance, which confirms the expectation from QRT calculations of the spectra.

Owing to the linearity of the master equation, the QRT yields the average of the correlation functions and hence the spectra. However, it does not reproduce the nonlinear procedure of fitting individual spectra by a Lorentzian to estimate the frequency. Our trajectory simulations within the second-order mean-field approach thus offer both qualitative insights into the dynamics, the role of the measurement noise and backaction, and a quantitative assessment of a practical procedure for frequency extraction from the emitted light.

In this Letter, we focused on calcium atoms incoherently pumped to the short-lived excited state, as studied in experiments [18]. As a result, the calculated power spectrum is broad, and the frequency precision is comparable with one of commercial microwave cesium clocks [3]. By exploring longer lived excited states of calcium atoms [33] or other species, like strontium atoms [13], we expect that the performance can be further improved by orders of magnitude and reach 2.4×10^{-16} with one second measurements [Fig. S11 of the Supplemental Material [19]]. Further work will then be needed to clarify the precise relationship between the frequency measurement performance and the incoherent pumping rate. During submission of the current work, we became aware of an experiment reporting the dynamical evolution of the heterodyne spectrum of the quasi-steady-state superradiance from incoherently pumped strontium-88 atoms [34]. We anticipate that our theoretical description may be applied to estimate the performance of such a system as a potential active optical clock.

Acknowledgments—This work was supported by the National Natural Science Foundation of China through Project No. 62027816, the Cross-Disciplinary Innovative Research Group Project of Henan Province No. 232300421004, and by the Carlsberg Foundation through the "Semper Ardens" Research Project QCooL.

[1] B. Jaduszliwer and J. Camparo, Past, present and future of atomic clocks for GNSS, GPS Solut. **25**, 27 (2021).
[2] J. C. Hafele and E. K. Richard, Around-the-world atomic clocks: Predicted relativistic time gains, Science **177**, 166 (1972).
[3] A. Bauch, Caesium atomic clocks: Function, performance and applications, Meas. Sci. Technol. **14**, 1159 (2003).
[4] A. D. Ludlow, M. M. Boyd, J. Ye, E. Peik, and P. O. Schmidt, Optical atomic clocks, Rev. Mod. Phys. **87**, 637 (2015).
[5] H. Katori, Optical lattice clocks and quantum metrology, Nat. Photonics **5**, 203 (2011).
[6] D. Meiser, J. Ye, D. R. Carlson, and M. J. Holland, Prospects for a millihertz-linewidth laser, Phys. Rev. Lett. **102**, 163601 (2009).
[7] D. A. Tieri, M. Xu, D. Meiser, J. Cooper, and M. J. Holland, Theory of the crossover from lasing to steady state superradiance, arXiv:1702.04830.
[8] K. Debnath, Y. Zhang, and K. Mølmer, Lasing in the superradiant crossover regime, Phys. Rev. A **98**, 063837 (2018).
[9] Y. Zhang, C. X. Shan, and K. Mølmer, Ultranarrow superradiant lasing by dark atom-photon dressed states, Phys. Rev. Lett. **126**, 123602 (2021).
[10] J. G. Bohnet, Z. Chen, J. M. Weiner, D. Meiser, M. J. Holland, and J. K. Thompson, A steady-state superradiant laser with less than one intracavity photon, Nature (London) **484**, 78 (2012).
[11] M. A. Norcia, M. N. Winchester, J. R. K. Cline, and J. K. Thompson, Superradiance on the millihertz linewidth strontium clock transition, Sci. Adv. **2**, e1601231 (2016).
[12] M. A. Norcia and J. K. Thompson, Cold-strontium laser in the superradiant crossover regime, Phys. Rev. X **6**, 011025 (2016).
[13] M. A. Norcia, J. R. K. Cline, J. A. Muniz, J. M. Robinson, R. B. Hutson, A. Goban, G. E. Marti, J. Ye, and J. K. Thompson, Frequency measurements of superradiance from the strontium clock transition, Phys. Rev. X **8**, 021036 (2018).
[14] C. Gardiner and P. Zoller, *Quantum Noise: A Handbook of Markovian and Non-Markovian Quantum Stochastic Methods with Applications to Quantum Optics* (Springer, Berlin, Heidelberg, 2004).
[15] R. J. Glauber, The quantum theory of optical coherence, Phys. Rev. **130**, 2529 (1963).
[16] Q. Xu, E. Greplova, B. Julsgaard, and K. Mølmer, Correlation functions and conditioned quantum dynamics in photodetection theory, Phys. Scr. **90**, 128004 (2015).
[17] D. P. Hansen, J. R. Mohr, and A. Hemmerich, Magnetic trapping of metastable calcium atoms, Phys. Rev. A **67**, 021401(R) (2003).
[18] T. Laske, H. Winter, and A. Hemmerich, Pulse delay time statistics in a superradiant laser with calcium atoms, Phys. Rev. Lett. **123**, 103601 (2019).

[19] See Supplemental Material at http://link.aps.org/supplemental/10.1103/PhysRevLett.133.073601 for additional details, which includes Refs. [3,6,8,18,20–24].
[20] C. Hotter, D. Plankensteiner, G. Kazakov, and H. Ritsch, Continuous multi-step pumping of the optical clock transition in Alkaline-earth atoms with minimal perturbation, Opt. Express **30**, 5553 (2022).
[21] Y. Zhang, C. X. Shan, and K. Mølmer, Active frequency measurement on superradiant strontium clock transitions, Phys. Rev. Lett. **128**, 013604 (2022).
[22] D. Plankensteiner, C. Hotter, and H. Ritsch, QuantumCumulants.jl: A Julia framework for generalized mean-field equations in open quantum systems, Quantum **6**, 617 (2022).
[23] H. W. Wiseman and G. J. Milburn, *Quantum Measurement and Control* (Cambridge University Press, Cambridge, England, 2010).
[24] D. W. Allan, Time and frequency (the-domain) characterization, estimation, and prediction of precision clocks and oscillators, IEEE Trans. Ultrason. Ferroelectr. Freq. Control **34**, 647 (1987).
[25] A. Gogyan, G. Kazakov, M. Bober, and M. Zawada, Characterisation and feasibility study for superradiant lasing in ^{40}Ca atoms, Opt. Express **28**, 6881 (2020).
[26] R. H. Dicke, Coherence in spontaneous radiation processes, Phys. Rev. **93**, 99 (1954).
[27] Y. Zhang, Y. X. Zhang, and K. Mølmer, Monte-Carlo simulations of superradiant lasing, New J. Phys. **20**, 112001 (2018).
[28] N. Shammah, S. Ahmed, N. Lambert, S. De Liberato, and F. Nori, Open quantum systems with local and collective incoherent processes: Efficient numerical simulations using permutational invariance, Phys. Rev. A **98**, 063815 (2018).
[29] J. C. MacGillivray and M. S. Feld, Theory of superradiance in an extended, optically thick medium, Phys. Rev. A **14**, 1169 (1976).
[30] D. Polder, M. F. H. Schuurmans, and Q. H. F. Vrehen, Superfluorescence: Quantum-mechanical derivation of Maxwell-Bloch description with fluctuating field source, Phys. Rev. A **19**, 1192 (1979).
[31] E. Bohr, S. L. Kristensen, C. Hotter, S. A. Schäffer, J. Robinson-Tait, J. W. Thomsen, T. Zelevinsky, H. Ritsch, and J. H. Müller, Collectively enhanced Ramsey readout by cavity sub- to superradiant transition, Nat. Commun. **15**, 1084 (2024).
[32] C. Hotter, L. Ostermann, and H. Ritsch, Cavity sub- and superradiance for transversely driven atomic ensembles, Phys. Rev. Res. **5**, 013056 (2023).
[33] A. V. Taichenachev, V. I. Yudin, C. W. Oates, C. W. Hoyt, Z. W. Barber, and L. Hollberg, Magnetic field-induced spectroscopy of forbidden optical transitions with application to lattice-based optical atomic clocks, Phys. Rev. Lett. **96**, 083001 (2006).
[34] S. L. Kristensen, E. Bohr, J. Robinson-Tait, T. Zelevinsky, J. W. Thomsen, and J. H. Müller, Subnatural linewidth superradiant lasing with cold ^{88}Sr atoms, Phys. Rev. Lett. **130**, 223402 (2023).